Vacuum Ultraviolet Pulsed Field Ionization−Photoelectron Study for N_2O^+ in the Energy Range of 16.3−21.0 eV†

Wenwu Chen and Jianbo Liu

Chemical Sciences Division, Lawrence Berkeley National Laboratory, Berkeley, California 94720

C. Y. Ng*

Department of Chemistry, University of California at Davis, One Shields Avenue, Davis, California 95616

Received: November 7, 2002; In Final Form: January 31, 2003

The vacuum ultraviolet pulsed field ionization−photoelectron (PFI−PE) spectra for N_2O have been measured in the energy range of 16.3−21.0 eV, covering the vibronic bands of $N_2O^+(A^2\Sigma^+$, $B^2\Pi$, and $C^2\Sigma^+)$. Many vibronic bands, which were not resolved in previous photoelectron studies, are identified in the present measurement. As observed in the HeI photoelectron spectra of N_2O, the PFI−PE spectra for $N_2O^+(A^2\Sigma^+$ and $C^2\Sigma^+)$ are dominated by excitation of the ν_1^+ (symmetric stretching) and ν_3^+ (antisymmetric stretching) modes, along with weak bands due to excitation of both even and odd quanta of the ν_2^+ (bending) mode. The simulation of the rotational contours resolved in the PFI−PE bands associated with excitation to $N_2O^+(A^2\Sigma^+$, $\nu_1^+ = 0-1$, $\nu_2^+ = 0$, and $\nu_3^+ = 0-1)$ has revealed the orbital angular momentum of the outgoing photoelectrons and yielded accurate ionization energies for the formation of these states from $N_2O(X^1\Sigma^+)$.

I. Introduction

As one of the linear triatomic molecules, N_2O and its cation have been extensively investigated by many experimental techniques, such as absorption,[1−5] emission,[6−9] fast ion beam laser spectroscopy,[10,11] photoelectron,[12−24] photoionization[25,26] and photodissociation,[27,28] and photoelectron−photoion coincidence spectroscopy.[22,29−32] Among these experimental studies, the photoelectron spectroscopic measurements [including HeI,[12−20] threshold photoelectron (TPE),[21,22] and pulsed filed ionization−photoelectron (PFI−PE)[23,24]], together with the theoretical investigations,[33,34] have provided the most information on the vibronic structures of N_2O^+. Previous HeI and TPE studies of N_2O have yielded reliable ionization energies (IEs) for the formation of many vibrational levels of the first four valence states $N_2O^+(X^2\Pi$, $A^2\Sigma^+$, $B^2\Pi$, and $C^2\Sigma^+)$ and have revealed many complex spectroscopic features, arising from spin−orbit couplings, Fermi resonances, and the Herzberg−Teller and Renner−Teller interactions associated with excitation of the bending (ν_2^+) mode for $N_2O^+(X^2\Pi)$. The observation of symmetry-forbidden excitation involving one quantum of the bending mode is noted in particular, indicative of vibronic couplings.

Using the coherent vacuum ultraviolet (vacuum-UV) laser PFI−PE measurement scheme, the photoelectron bands associated with excitation to $N_2O^+(X^2\Pi$, $\nu_1^+ = 0-1$, $\nu_2^+ = 0-2$, and $\nu_3^+ = 0)$ and $N_2O^+(A^2\Sigma^+$, $\nu_1^+ = 0-1$, $\nu_2^+ = 0$, and $\nu_3^+ = 0)$ have been examined at a resolution of 2−5 cm^{-1} (full-width at half-maximum, fwhm),[23,24] allowing the observation of rotational structures. Here, ν_1^+ and ν_3^+ represent the respective symmetric and antisymmetric stretching modes for N_2O^+. The adiabatic IEs for the formation of $N_2O^+(X^2\Pi_{3/2}$, $X^2\Pi_{1/2}$, and $A^2\Sigma^+)$ [IE($N_2O^+(X^2\Pi_{3/2}$,$X^2\Pi_{1/2}$,and$A^2\Sigma^+)$] determined in the vacuum-UV laser PFI−PE experiments by Wiedmann et al.[23] and Kong et al.[24] are 103 963 ± 5, 104 097 ± 5, and 132 191 ± 2 cm^{-1}, respectively. The rotational analysis of each vibronic band has revealed valuable dynamical information, such as angular momentum transfer during photoionization, rotational and spin−orbit autoionizing mechanisms, and effects of predissociation. However, because of the difficulty in generating a wide tunable photon energy range using the vacuum-UV laser sources, the previous PFI−PE studies on N_2O were only made in very narrow photon energy ranges (i.e., 12.87−13.05 [23] and 16.38−16.56 eV [24]).

Recently, we have developed a synchrotron-based scheme for PFI−PE measurement[35] by using a high-resolution vacuum-UV monochromatized undulator synchrotron source (photon energy range = 6−30 eV) at the Chemical Dynamics Beamline of the Advance Light Source (ALS).[36,37] The synchrotron-based PFI−PE scheme can achieve a resolution similar to that attained in laser-based studies. The most attractive feature of the synchrotron radiation is its ease of tunability, making high-resolution PFI−PE measurement for many molecules in a large energy region a routine operation. Using the high-resolution synchrotron-based PFI−PE technique, we have obtained the rotationally resolved PFI−PE spectra for many diatomic molecules[38−40] and linear triatomic molecules CO_2,[41−43] CS_2,[44,45] and OCS.[46,47]

In this paper, we present a synchrotron-based PFI−PE study for N_2O in the energy region of 16.3−21.0 eV, covering the ionization transitions from $N_2O(X^1\Sigma^+)$ to valence ionic states $N_2O^+(A^2\Sigma^+$, $\nu_1^+ = 0-4$, $\nu_2^+ = 0-2$, and $\nu_3^+ = 0-2)$, N_2O^+-$(B^2\Pi)$, and $N_2O^+(C^2\Sigma^+$, $\nu_1^+ = 0-3$, $\nu_2^+ = 0-2$, and $\nu_3^+ = 0-2)$. As shown below, the present PFI−PE measurement reveals many new vibronic features, which were not resolved in previous HeI and TPE measurements. Furthermore, we have resolved rotational contours for selected vibrational PFI−PE bands for $N_2O^+(A^2\Sigma^+)$. The simulation of these rotational

† Part of the special issue "A. C. Albrecht Memorial Issue".

* To whom correspondence should be addressed. E-mail: cyng@chem.ucdavis.edu.

10.1021/jp022389d CCC: $25.00
Published on Web 04/11/2003

contours has provided accurate IE values for $N_2O^+(A^2\Sigma^+, \nu_1^+ = 0-1, \nu_2^+ = 0$, and $\nu_3^+ = 0-1)$.

II. Experiment and Simulation

A. Experiment. The experiment was carried out using the photoelectron−photoion apparatus of the Chemical Dynamics Beamline at the ALS.[35−37] In the present experiment, helium (pressure ≈ 25 Torr) was used in the harmonic gas filter to suppress higher undulator harmonics with photon energies greater than 24.58 eV. Undulator light of the first harmonic emerging from the gas filter was directed into the 6.65m Eagle monochromator and dispersed by an Os-coated, 4800 line/mm grating (dispersion = 0.32 Å/mm) before entering the photoionization−photoexcitation (PI/PEX) region of the photoelectron−photoion apparatus. The monochromator entrance/exit slits used vary in the range of 30/30 to 400/400 μm, which corresponds to nominal wavelength resolution in the range of 0.010−0.128 Å (fwhm).

The N_2O sample obtained from Aldrich, was introduced into the PI/PEX region as a continuous, neat N_2O molecule beam by the supersonic expansion through a stainless steel nozzle (diameter = 0.127 mm; stagnation temperature = 298 K; stagnation pressure ≈ 760 Torr) and was skimmed by a conical skimmer before intersecting the dispersed vacuum-UV photon beam 7 cm downstream in the PI/PEX region. The pressure in the photoionization chamber was maintained at $\sim 2 \times 10^{-6}$ Torr during the experiment.

The procedures for synchrotron-based PFI−PE measurements have been described in detail previously.[35] This scheme takes advantage of the dark gap (48 ns) existing between adjacent synchrotron ring periods for the application of the pulsed electric field for PFI. The pulsed electric field (1.5 V/cm, 40 ns) was applied by 8 ns delay with respect to the beginning of the 48 ns dark gap, and the time interval between adjacent PFI pulses was 1.312 μs, which was equal to two synchrotron ring periods. A higher resolution measurement was made using a PFI field of 0.5 V/cm for selected PFI−PE bands.

The PFI−PE intensities presented here were normalized by the corresponding vacuum-UV photon intensities, which were monitored using a calibrated tungsten photoelectric detector.[48] The energy step sizes used were in the range of 0.1−0.5 meV, and the counting times for each step varied in the range of 4−8 s. All PFI−PE spectra were calibrated before and after each experiment using the $Ar^+(^2P_{3/2})$ and $Ne^+(^2P_{3/2})$ PFI−PE bands obtained under the same experimental conditions.[35,37] The calibration scheme assumes that the Stark shifts of the IEs of N_2O and rare gases are identical. Previous measurements indicate that the uncertainty of this calibration method is within ± 0.5 meV.[38−47]

B. Simulation of Rotational Transition Intensities in PFI−PE Bands. In an effort to interpret the rotational contours observed in the high-resolution PFI−PE bands associated with $A^2\Sigma^+(0_0^0)$, $A^2\Sigma^+(1_0^1)$, $A^2\Sigma^+(3_0^1)$, and $A^2\Sigma^+(1_0^13_0^1)$, simulation was performed using the Buckingham−Orr−Sichel (BOS) model.[49] This model was derived to predict relative transition line strengths observed in single-photon ionization of diatomic molecules, and can be extended to that of linear molecules in the photoionization process.[23,24,41−45] The BOS rotational line strength $\sigma_{J^+\leftarrow J''}$ could be expressed as a sum of terms in the orbital angular momentum l of the outgoing electron:

$$\sigma_{J^+\leftarrow J''} \propto \sum_{\lambda} C_\lambda Q(\lambda, J'', J^+) \qquad (1)$$

where J'' and J^+ are the total angular momentum for the neutral and ionic states, respectively. The BOS coefficients C_λ are linear combinations of electron transition amplitudes for the possible orbital angular momentum l of the ejected electron. $Q(\lambda, J'', J^+)$ is the Clebsch−Gordon coefficients determined by the standard angular momentum coupling constants, which take different forms depending on the Hund's coupling case for neutral and ionic states.[50] The parameter λ is the quantum number related to the orbital angular momentum transferred to the ion core and is restricted by

$$l - 1 \le \lambda \le l + 1 \qquad (2)$$

The ionizing transition $N_2O^+(A^2\Sigma^+) \leftarrow N_2O(X^1\Sigma^+)$ belongs to the simplest case in the BOS model, in which both the neutral and ionic states could be described as Hund's coupling case (b).[50] The initial and the final states could be described by the projection of the electronic orbital angular momentum (Λ'', Λ^+) onto the molecular axis, the total angular momentum (J'', J^+), and the total spin (S'', S^+), where the double primes and pluses refer to the neutral and ionic states, respectively. The Clebsch−Gordon coefficients $Q(\lambda, J'', J^+)$ could be simplified as

$$Q(\lambda, J'', J^+) = (2J'' + 1)^2 \begin{pmatrix} J'' & \mathrm{l} & J^+ \\ -\Lambda'' & \Delta\mathrm{L} & \Lambda^+ \end{pmatrix} \qquad (3)$$

where $\Delta\Lambda = \Lambda^+ - \Lambda''$. Since $\Lambda^+ = \Lambda'' = 0$ for the ionic and neutral Σ states, the three-J symbol in eq 3 will be nonzero only when $J^+ + \mathrm{l} + J'' =$ even and $|J^+ - J''| \le \mathrm{l}$. This indicates that, for the $^2\Sigma^+ \leftarrow {}^1\Sigma^+$ transition, the *s*-wave character ($\lambda = 0$) will contribute only to the Q-rotational branch, *p*-wave character ($\lambda = 1$) to the P- and R-rotational branches, *d*-wave character ($\lambda = 2$) to the O-, Q- and S-branches, and *f*-wave character ($\lambda = 3$) to the N-, P-, R-, and T-branches, etc.

The simulation used the rotational constant $B'' = 0.4190$ cm^{-1} for the neutral ground-state $N_2O(X^1\Sigma^+)$,[51] and the B^+ values used for various vibrational states of $N_2O^+(A^2\Sigma^+)$ were taken from refs 6 and 9. A Gaussian instrumental profile (fwhm = 5 cm^{-1}) was used to simulate the observed rotational contours. Simulation was performed by varying the rotational temperature and making estimates for the coefficients C_λ until a best fit was obtained. We found that a rotational temperature of 200−300 K for N_2O gave the best fits for the experimental PFI−PE bands. The high rotational temperature of N_2O or lack of cooling observed in the present experiment is most likely due to a misalignment problem of the supersonic beam production system.[43] We limited the orbital angular momentum of the photoelectron to $l \le 3$ in simulation since high l values are not expected to have significant contributions due to the high centrifugal barrier at the threshold. This restriction results in $\lambda = 0-4$. We found that in most cases only C_λ ($\lambda = 0-2$) are actually needed in the fits, indicating that the PFI−PE bands are mostly attributed to nsσ, npσ, npπ, ndσ, and ndπ Rydberg series converging to $N_2O^+(A^2\Sigma^+)$, with orbital angular momentum $l \le 2$. Since the small spin-rotation interaction (Λ double splitting) cannot be resolved in the present experiment, individual ± parity (F1/F2) levels are viewed as degenerate in the simulation.

III. Results and Discussion

The neutral ground-state $N_2O(X^1\Sigma^+)$ is isoelectronic with CO_2, with 22 electrons and a linear geometry. Its dominant electronic configuration is $(1\sigma)^2(2\sigma)^2(3\sigma)^2(4\sigma)^2(5\sigma)^2(6\sigma)^2(1\pi)^4(7\sigma)^2(2\pi)^4$. The vibrational frequencies ν_1'' (symmetry stretching), ν_2'' (bending), and ν_3'' (anti-symmetric stretching) of

TABLE 1: Ionization Energies (IEs), Relative Intensities, and Vibronic Assignments of PFI−PE Bands for $N_2O^+(A^2\Sigma^+)$

IE[a,b] (eV)	ΔE[a,b] (cm^{-1})	assignment	rel intens[c] PFI[a]	TPE[b]	HeI[d]
16.3905 [e] (16.391)	0	$(0,0,0)^2\Sigma^+ \leftarrow (0,0,0)^1\Sigma^+$	100.0	100.0	100.0
16.4662	611	$(0,1,0)^2\Pi \leftarrow (0,0,0)^1\Sigma^+$	1.0		2.1
16.5414	1217	$(0,2,0)^2\Sigma^+ \leftarrow (0,0,0)^1\Sigma^+$	2.7		
16.5574 [e] (16.560)	1346 (1360)	$(1,0,0)^2\Sigma^+ \leftarrow (0,0,0)^1\Sigma^+$	41.2	39.5	21.7
16.6346	1969	$(1,1,0)^2\Pi \leftarrow (0,0,0)^1\Sigma^+$	0.5		1.1
16.6943 [e] (16.698)	2450 (2475)	$(0,0,1)^2\Sigma^+ \leftarrow (0,0,0)^1\Sigma^+$	9.5	10.8	8.5
16.7059	2544	$(1,2,0)^2\Sigma^+ \leftarrow (0,0,0)^1\Sigma^+$	1.2		
16.7221 (16.728)	2675 (2715)	$(2,0,0)^2\Sigma^+ \leftarrow (0,0,0)^1\Sigma^+$	4.5	7.3	0.5
16.8575 [e] (16.864)	3767 (3815)	$(1,0,1)^2\Sigma^+ \leftarrow (0,0,0)^1\Sigma^+$	2.9	~2	1.0
16.8861 (16.892)	3997 (4035)	$(3,0,0)^2\Sigma^+ \leftarrow (0,0,0)^1\Sigma^+$	1.4	~1	0.1
16.9942	4869	$(0,0,2)^2\Sigma^+ \leftarrow (0,0,0)^1\Sigma^+$	1.2		0.5
17.0178	5060	$(2,0,1)^2\Sigma^+ \leftarrow (0,0,0)^1\Sigma^+$	0.7		
17.0496	5316	$(4,0,0)^2\Sigma^+ \leftarrow (0,0,0)^1\Sigma^+$	0.6		

[a] This work. Here ΔE values are energies measured with respect to the IE[$A^2\Sigma^+(0_0^0)$]. [b] The values in parentheses are given in ref 21. [c] The intensity for the origin band $^2\Sigma^+(0_0^0)$is arbitrarily set to 100. [d] Reference 8. [e] IE determined by BOS simulation.

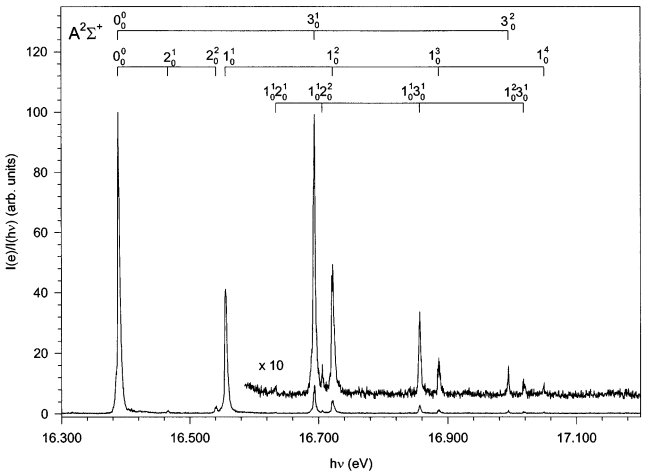

Figure 1. PFI−PE spectrum for the $N_2O^+(A^2\Sigma^+)$ state in the energy range of 16.30−17.20 eV obtained at a PFI−PE resolution of 7 cm^{-1} (fwhm).

$N_2O(X^1\Sigma^+)$ are known to be 1284.9, 588.8, and 2223.8 cm^{-1}, respectively.[51] Removing an electron from the 7σ, 1π, or 6σ orbital results in $N_2O^+(A^2\Sigma^+, B^2\Pi$, or $C^2\Sigma^+)$, respectively. The respective vibrational frequencies ν_1^+, ν_2^+, and ν_3^+ of N_2O^+-$(A^2\Sigma^+)$ are listed as 1345.5, 614, and 2451.7 cm^{-1} in Herzberg.[51] We note that although $N_2O^+(A^2\Sigma^+$ and $C^2\Sigma^+)$ states are both formed by removal of a σ electron from the neutral, they have different characters. The 7σ orbital, with dominant contributions from the 2s and 2p orbitals of the N atoms, has more nonbonding character than the 6σ orbital, which is mainly composed of the 2s and $2p_z$ orbitals of the O and N atoms. This difference is expected to give rise to different characters of Rydberg series, which converge to the $N_2O^+(A^2\Sigma^+$ and $C^2\Sigma^+)$ states, and thus might result in different intensity distributions in the PFI−PE spectra for $N_2O^+(A^2\Sigma^+$ and $C^2\Sigma^+)$.

A. PFI−PE Spectrum for $N_2O^+(A^2\Sigma^+)$. Figure 1 shows the PFI−PE spectrum for $N_2O^+(A^2\Sigma^+)$ in the energy region of 16.3−17.2 eV, taken at a PFI−PE resolution of 7 cm^{-1}. The IEs, relative intensities, and assignments for the PFI−PE bands resolved in Figure 1 are summarized in Table 1. For comparison, we have also included in Table 1 the peak positions and relative intensities of vibronic bands resolved in HeI study of Dehmer et al.[18] and TPE study of Frey et al.[21] As shown in Table 1, the main spectroscopic features observed in the present PFI−PE study are similar to those observed in HeI and TPE measurements. However, the high-resolution PFI−PE measurement

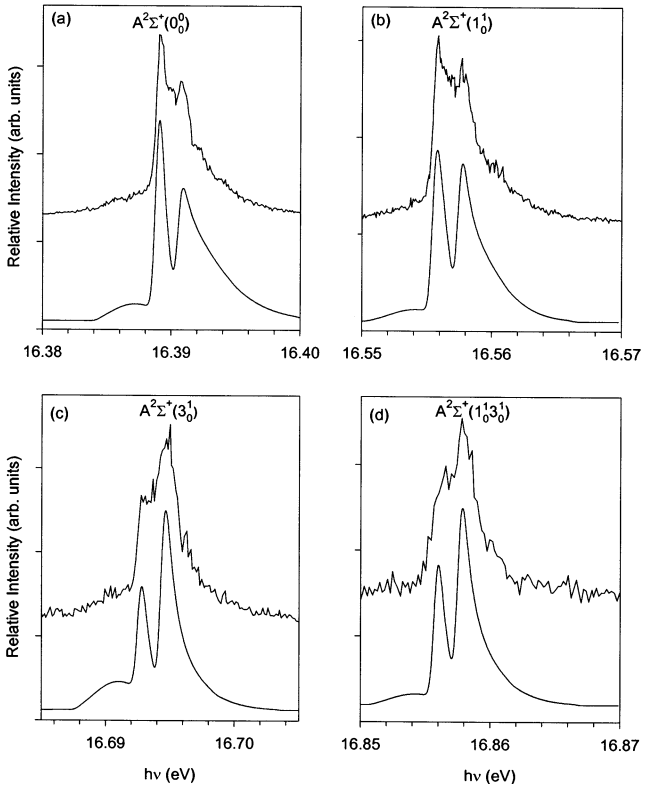

Figure 2. Comparison of the PFI−PE spectrum (top) and the BOS simulated spectrum (bottom) for (a) $A^2\Sigma_u^+(0_0^0)$ in the energy range of 16.38−16.40 eV, (b) $A^2\Sigma_u^+(1_0^1)$ in the energy range of 16.55−16.57 eV, (c) $A^2\Sigma_u^+(3_0^1)$ in the energy range of 16.685−16.705 eV, and (d) $A^2\Sigma_u^+(1_0^13_0^1)$ in the energy range of 16.85−16.87 eV. PFI−PE resolution = 4 cm^{-1} (fwhm).

reveals many new vibronic bands, which were not observed in previous photoelectron studies, and makes the assignments more reliable.

The $N_2O^+(A^2\Sigma^+)$ state is also known to be linear with its respective equilibrium N−N distance R_{N-N} (=1.140 Å) and N−O distance R_{N-O} (=1.141 Å) close to those of 1.1266 and 1.1856 Å for $N_2O(X^1\Sigma^+)$.[6] This is in agreement with the nonbonding character of the 7σ orbital. The similar geometries for $N_2O^+(A^2\Sigma^+)$ and $N_2O(X^1\Sigma^+)$ result in the overwhelming Franck−Condon factor for the origin band $A^2\Sigma^+(0_0^0)$.

Figure 2a shows the high-resolution PFI−PE spectrum (top spectrum) for the $A^2\Sigma^+(0_0^0)$ band obtained at a PFI−PE resolution of 4 cm^{-1} (fwhm), exhibiting a sharp peak followed

by a broad peak at high energy. In addition, a weak and broad shoulder is discernible at the low-energy side of the spectrum. Although it is not possible to resolve individual rotational transitions for $A^2\Sigma^+(0_0^0)$, which has a rotational constant of $B^+ = 0.433$ cm^{-1}, the observed features can clearly be attributed to the rotational contours of the PFI−PE band for $A^2\Sigma^+(0_0^0)$. The simulated spectrum (bottom spectrum in Figure 2a) for the $A^2\Sigma^+(0_0^0)$ band was obtained using the rotational constants B'' = 0.4190 cm^{-1} for $N_2O(X^1\Sigma^+)$ and $B^+ = 0.4340$ cm^{-1} for $N_2O^+(A^2\Sigma^+)$.[6,9−11] The BOS coefficients C_λ ($\lambda = 0-4$) used in this simulation are $C_0 = 0.15$, $C_1 = 0.58$, $C_2 = 0.27$, and $C_3 = C_4 = 0$, respectively. As shown in Figure 2a, the simulated spectrum reproduces the experimental band quite well. On the basis of the BOS simulation, we could assign the rotational features in the PFI−PE band to different rotational transition branches. The BOS coefficients $C_3 = C_4 = 0$ indicate that only the transitions with $\Delta J = 0, \pm 1$, and ± 2 need to be taken into account. The sharp peak around 16.389 eV is assigned as the P-branch ($\Delta J = -1$), and the broad peak at 19.391 eV is attributed to the combination of the Q- ($\Delta J = 0$) and R-branches ($\Delta J = 1$). The weak band below 16.388 eV can be attributed to the O-branch ($\Delta J = -2$). There exists a less-resolved broad band at even higher energy, indicating the possible contribution from the S-branch ($\Delta J = 2$) transitions. The contributions from higher $|\Delta J| > 2$ transitions are found to be negligibly small. The rotational contours of $A^2\Sigma^+(0_0^0)$ is asymmetric with the $\Delta J < 0$ branches more pronounced relative to the $\Delta J > 0$ branches. These asymmetric structures can be ascribed to the perturbation by rotational autoionization.[52]

The Rydberg series converging to $(0,0,0)A^2\Sigma^+$ are nsσ, npσ, npπ, ndσ, and ndπ in nature,[25] with ns states formed from a p-orbital, np from a s- and/or a d-orbital, and ndπ from a p- and/or a f-orbital. The dominance of the P- and R-branches in the present PFI−PE spectrum is indicative of the p-orbital character in the initial state. This conclusion is different than that of the previous PFI−PE spectrum by Kong et al.[24] In the latter experiment, the main contribution for the $A^2\Sigma^+(0_0^0)$ band was found to come from the N-, Q-, and T-branches, indicating that the initial state has the d- and f-orbital characters. The major difference between the two PFI−PE experiments is that the rotational temperature achieved in Kong et al.'s was much lower (estimated as 10 K). Thus, it could be inferred that the PFI−PE band for $A^2\Sigma^+(0_0^0)$ is mediated by the ns and nd Rydberg series at high rotational temperatures and by np and nd at low rotational temperatures. On the basis of the BOS simulation, we deduce the IE$[A^2\Sigma^+(0_0^0)] = 16.3905 \pm 0.0005$ eV (132 198 $\pm$ 4 cm^{-1}), which is consistent with that of 16.3896 eV (132 191 cm^{-1}) determined from the laser-based PFI−PE measurement of Kong et al.[24] and 16.3914 eV (132 205 cm^{-1}) determined in the previous TPE study of Frey et al.[21] The value of 16.388 eV (132 178 cm^{-1}) obtained from the extrapolation of the Rydberg series by Berkowitz et al. is slightly lower.[25]

The prominent vibrational bands for $N_2O^+(A^2\Sigma^+)$ in the PFI−PE spectrum are attributed to excitation of the ν_1^+ mode. These bands appear as $^2\Sigma^+(1_0^1)$ at 16.5574 eV, $^2\Sigma^+(1_0^2)$ at 16.7221 eV, $^2\Sigma^+(1_0^3)$ at 16.8861 eV, and $^2\Sigma^+(1_0^4)$ at 17.0496 eV. The high-resolution PFI−PE spectrum for $^2\Sigma^+(1_0^1)$ (top spectrum) with its BOS simulation (bottom spectrum) are shown in Figure 2b. The simulated spectrum was obtained with the following parameters: $C_0 = 0.20$, $C_1 = 0.60$, $C_2 = 0.20$, and $C_3 = C_4 = 0$. The rotational profiles of $^2\Sigma^+(1_0^1)$ are similar to those of $^2\Sigma^+(0_0^0)$. Two prominent peaks can be attributed to the P-branch and the combination of the Q- and R-branches, respectively. Furthermore, broad O- and S-branches are resolved at low- and high-energy sides, respectively. Again, due to rotational autoionization, the P-branch appears enhanced in the PFI−PE spectrum compared to the simulation. The IE$[A^2\Sigma^+(1_0^1)]$ deduced from the BOS simulation is 16.5574 $\pm$ 0.0005 eV (133 544 $\pm$ 4 cm^{-1}), which is also in agreement with the laser-based PFI−PE value of 16.5562 eV (133 535 cm^{-1}).[24]

The excitations of 1 and 2 quanta of ν_2^+ are observed, at 16.4662 eV [$^2\Pi(2_0^1)$] and 16.5412 eV [$^2\Sigma^+(2_0^2)$]. Although to the first-order approximation the vibrational excitation of an odd quantum of ν_2^+ is forbidden in the linear $^2\Sigma^+ \leftarrow {}^1\Sigma^+$ transition, the $^2\Pi(2_0^1)$ band has been observed in HeI and TPE studies[18,21] and has been attributed to the vibronic coupling with the $X^2\Pi$ state. The $^2\Sigma^+(2_0^2)$ band, which is a symmetry allowed transition, was not resolved in previous HeI and TPE studies probably because this band is too close to the strong PFI−PE band for $^2\Sigma^+(1_0^1)$. Note that the intensities of vibrational bands associated with $\nu_2^+ = 2$ are observed with considerable intensity. This may partially due to the Fermi resonance between (ν_1^+, 0, 0) and ($\nu_1^+ - 1$, $\nu_2^+ = 2$, 0) which allows ($\nu_1^+ - 1$, $\nu_2^+ = 2$, 0) to derive intensity from (ν_1^+, 0, 0). The Fermi resonance interaction between the (ν_1^+, 0, 0) and ($\nu_1^+ - 1$, $\nu_2^+ = 2$, 0) levels of $N_2O^+(X^2\Pi)$ has already been observed in previous HeI studies.[18] The vibrational bands resolved in the PFI−PE spectrum of Figure 1 also include the PFI−PE bands for $^2\Sigma^+(3_0^1)$ at 16.6943 eV and $^2\Sigma^+(1_0^2)$ at 16.9942 eV, which belong to members of the ν_3^+-progression. Figure 2c shows the high-resolution PFI−PE band for $^2\Sigma^+(3_0^1)$ (top spectrum). Using $B^+ = 0.432$ cm^{-1} and $C_0 = 0.23$, $C_1 = 0.33$, $C_2 = 0.44$, and $C_3 = C_4 = 0$, we have obtained a satisfactory BOS fit for this band (bottom spectrum of Figure 2c). The simulation of the PFI−PE band for $^2\Sigma^+(3_0^1)$ results in a value of 16.6943 $\pm$ 0.0005 eV (134 649 $\pm$ 4 cm^{-1}) for the IE$[^2\Sigma^+(3_0^1)]$. Contrary to those for the $^2\Sigma^+(0_0^0)$ and $^2\Sigma^+(1_0^1)$ bands, the higher *l*-orbitals give more contributions for the $^2\Sigma^+(3_0^1)$ band; i.e., the contribution from p-orbital ($\lambda = 1$) decreases, while the contributions from s- ($\lambda = 0$) and d- ($\lambda = 2$) orbitals increase. The $^2\Sigma^+(3_0^1)$ band also contains higher ΔJ transitions components, e.g. O- and S-branches.

In addition to the overtones of ν_1^+, ν_2^+, and ν_3^+, combination bands are clearly resolved, which include $^2\Pi(1_0^1 2_0^1)$ at 16.6346 eV, $^2\Sigma^+(1_0^1 2_0^2)$ at 16.7059 eV, $^2\Sigma^+(1_0^1 3_0^1)$ at 16.8575 eV, and $^2\Sigma^+(1_0^2 3_0^1)$ at 17.0178 eV. The assignment of $^2\Pi(1_0^1 2_0^1)$ at 16.634 eV in the HeI study of Dehmer et al.[18] was made as tentative, because of the interference from impurity peak in HeI. This assignment was confirmed in the present PFI−PE measurement. High-resolution PFI−PE band for $^2\Sigma^+(1_0^1 3_0^1)$ (top spectrum) is compared to the simulated spectrum (bottom spectrum) in Figure 2d obtained using $B^+ = 0.432$ cm^{-1} and $C_0 = 0.31$, $C_1 = 0.41$, $C_2 = 0.18$, $C_3 = 0.10$, and $C_4 = 0$. The rotational contours appearing in the spectrum are similar to those for $^2\Sigma^+(3_0^1)$, which indicates the dominance in the excitation of the ν_3^+ mode in the PFI−PE spectrum. The simulation of $^2\Sigma^+(1_0^1 3_0^1)$ indicates that higher ΔJ transitions contribute to the band. Besides the $|\Delta J| \leq 2$ transitions, which exist in the $^2\Sigma^+(0_0^0)$, $^2\Sigma^+(1_0^1)$, and $^2\Sigma^+(3_0^1)$, $\Delta J = \pm 3$ transitions also exist in the $^2\Sigma^+(1_0^1 3_0^1)$ band. The simulation yields an IE$[^2\Sigma^+(1_0^1 3_0^1)]$ value of 16.8575 $\pm$ 0.0005 eV (135 965 $\pm$ 4 cm^{-1}).

The frequencies of ν_1^+, ν_2^+, and ν_3^+ for $N_2O^+(A^2\Sigma^+)$ deduced from the PFI−PE measurement are 1346, 611, and 2450 cm^{-1}, respectively. These values are in excellent agreement with $\nu_1^+ = 1346$ cm^{-1}, $\nu_2^+ = 614$ cm^{-1}, and $\nu_3^+ = 2452$ cm^{-1} from emission[6,21] and $\nu_1^+ = 1344$ cm^{-1} from laser-based PFI−PE measurement.[24] The values of $\nu_1^+ = 1360$ cm^{-1} and $\nu_3^+ = 2475$ cm^{-1} determined in the previous TPE study are likely too high.[21]

We have compared in Table 1 the relative intensities for the vibronic bands observed in the present PFI−PE measurement with those reported in the previous HeI[18] and TPE[21] studies. As expected, the intensities observed in the PFI−PE measurement are close to those in the TPE study, but quite different from those found in the HeI study, especially for those involving the ν_2^+ and ν_3^+ modes. For example, the intensity for $^2\Pi(2_0^1)$ band was 2.1% of the origin band in HeI but decreases to 1.0% in the PFI−PE spectrum; the intensity for $^2\Sigma^+(1_0^1)$ was 22% of the origin band in HeI, whereas in the PFI−PE and TPE spectra it increases to about 40%. It is well-known that the photoelectrons in HeI excitation are mostly due to direct photoionization, and their intensities are governed by the Franck−Condon factors for the formation of these states. The enhanced TPE and PFI−PE intensities result from the detection of near-threshold electrons, which are susceptible to perturbation of near-resonance autoionizing Rydberg states. Lindholm[3] predicted five Rydberg series (nsσ, npσ, npπ, ndσ, and ndπ) converging to the $N_2O^+(A^2\Sigma^+)$ state, which were identified later by photoabsorption[2] and photoionization measurements.[25] Furthermore, the intensities for PFI−PE bands observed in this synchrotron-based experiment depend on the lifetime effects of high-*n* Rydberg states involved because high-*n* Rydberg states initially prepared by vacuum-UV excitation are not expected to be fully stabilized.[36] The $N_2O^+(A^2\Sigma^+)$ state is known to fluorescence to the $N_2O^+(X^2\Pi)$ state[6−9] and except for the $(0,0,0)A^2\Sigma^+$ level, the higher vibrational level of $N_2O^+(A^2\Sigma^+)$ are predissociated.[30] The lifetimes of these vibrational levels are rather short (<240 ns).[7,30] Thus, fluorescence and predissociation should also be viable decay channels for excited N_2O in high-*n* Rydberg states converging to $N_2O^+(A^2\Sigma^+)$. The existence of these decay channels might also affect the band intensities in the PFI−PE spectrum. However, Kong et al.[24] reported that no significant changes in PFI−PE intensities were observed for a delay time up to 1.8 μs.

B. PFI−PE Spectrum for $N_2O^+(B^2\Pi)$. Similar to the vibronic structures observed in the previous HeI spectrum,[18] the PFI−PE spectrum for $N_2O^+(B^2\Pi)$ in the energy region of 17.4−19.0 eV (not shown here) displays a complex pattern of bands, consisting of a long series of broad peaks spreading over 1.5 eV. No simple vibrational progressions could be assigned for $N_2O^+(B^2\Pi)$. The theoretical investigation by Köppel et al.[34] suggested that the complex structure of the observed spectrum for $N_2O^+(B^2\Pi)$ is due to the interaction of two ionic states within this energy range. These two states are both the in-phase and out-of-phase linear combination of the $(1\pi)^{-1}$ single-hole and $(2\pi)^{-2}(3\pi)$ type pseudo states and interact vibronically through totally symmetric vibrational modes. With this assumption, they were able to reproduce the HeI photoelectron bands for $N_2O^+(B^2\Pi)$ by Green's function calculations. However, Cvitaš et al.[19] argued that the two-particle hole Tamm−Dancoff approximation to the Green's function used in Köppel et al.'s calculation was not extremely accurate. Alternatively, Cvitaš et al. explained the band in terms of the one electronic state Fermi resonance and Renner−Teller mixing. Both of these analyses are of somewhat empirical in nature, and a high-level theoretical investigation on $N_2O^+(B^2\Pi)$ state would be necessary to interpret the vibrational structures for $N_2O^+(B^2\Pi)$.

Due to the threshold nature of the PFI−PE detection scheme, some low-energy prompt electrons background from the autoionizing Rydberg series are observed in the Franck−Condon gap of 19.0−20.0 eV. The analysis of these Rydberg structures shows that these Rydberg states belong to members ($n = 4-13$) of the known Tanaka's series VII converging to $N_2O^+(C^2\Sigma^+)$ at 162 157 cm^{-1}.[2]

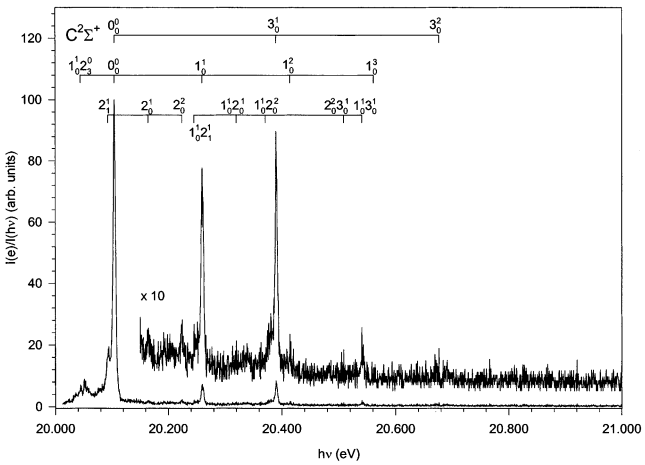

Figure 3. PFI−PE spectrum for the $N_2O^+(C^2\Sigma^+)$ state in the energy range of 20.00−21.00 eV obtained at a PFI−PE resolution of 7 cm^{-1} (fwhm).

TABLE 2: Ionization Energies (IEs), Relative Intensities, and Vibronic Assignments for the PFI−PE Bands of $N_2O^+(C^2\Sigma^+)$

IE[a] (eV)	$\Delta E^{a,b}$ (cm^{-1})	assignment	rel intens[c]
20.0443	−487	$(1,0,0)^2\Sigma^+ \leftarrow (0,3,0)^1\Pi$	1.8
20.0930	−94	$(0,1,0)^2\Pi \leftarrow (0,1,0)^1\Pi$	15
20.1047	0	$(0,0,0)^2\Sigma^+ \leftarrow (0,0,0)^1\Sigma^+$	100 (100)
20.1645	482 (508)	$(0,1,0)^2\Pi \leftarrow (0,0,0)^1\Sigma^+$	2.0 (0.9)
20.2244	965 (952)	$(0,2,0)^2\Sigma^+ \leftarrow (0,0,0)^1\Sigma^+$	2.3 (1.0)
20.2456	1136	$(1,1,0)^2\Pi \leftarrow (0,1,0)^1\Pi$	2.0
20.2598	1251 (1242)	$(1,0,0)^2\Sigma^+ \leftarrow (0,0,0)^1\Sigma^+$	7.3 (13.5)
20.3202	1738	$(1,1,0)^2\Pi \leftarrow (0,0,0)^1\Sigma^+$	1.0
20.3771	2197	$(1,2,0)^2\Sigma^+ \leftarrow (0,0,0)^1\Sigma^+$	2.0
20.3899	2300 (2283)	$(0,0,1)^2\Sigma^+ \leftarrow (0,0,0)^1\Sigma^+$	8.5 (18.7)
20.4145	2499	$(2,0,0)^2\Sigma^+ \leftarrow (0,0,0)^1\Sigma^+$	1.8
20.5088	3259	$(0,2,1)^2\Sigma^+ \leftarrow (0,0,0)^1\Sigma^+$	1.0
20.5406	3516 (3492)	$(1,0,1)^2\Sigma^+ \leftarrow (0,0,0)^1\Sigma^+$	2.1 (1.6)
20.5611	3681	$(3,0,0)^2\Sigma^+ \leftarrow (0,0,0)^1\Sigma^+$	0.9
20.6766	4613 (4565)	$(0,0,2)^2\Sigma^+ \leftarrow (0,0,0)^1\Sigma^+$	1.0 (<0.2)

[a] This work. Here ΔE values are energies measured with respect to the IE$[A^2\Sigma^+(0_0^0)]$. [b] The values in parentheses are given in ref 18. [c] The intensity for the origin band $^2\Sigma^+(0_0^0)$ is arbitrarily set to 100.

C. PFI−PE Spectrum for $N_2O^+(C^2\Sigma^+)$. The PFI−PE spectrum in the energy range of 20.0−21.0 eV is depicted in Figure 3 with marking of the assigned vibronic bands. Similar to the PFI−PE spectrum for $N_2O^+(A^2\Sigma^+)$, the PFI−PE spectrum for $N_2O^+(C^2\Sigma^+)$ is dominated by the overwhelming ionization transition $(0,0,0)C^2\Sigma^+ \leftarrow (0,0,0)X^1\Sigma^+$. The IEs, relative intensities, and assignments for the PFI−PE bands associated with $N_2O^+(C^2\Sigma^+)$ are listed in Table 2, together with the results of the HeI study by Dehmer et al.[18] As shown in the Figure 3 and Table 2, the improved resolution used in the present experiment has allowed the identification of many new vibronic bands.

The position of the $C^2\Sigma^+(0_0^0)$ band provides an IE value of 20.1047 ± 0.0005 eV (162 155 ± 4 cm^{-1}). The present value is inconsistent with the previous value of 20.105 eV (162 158 cm^{-1}) based on Rydberg series extrapolation,[25] the TPE value of 20.101 eV (162 125 cm^{-1}),[22] and the HeI value of 20.11 eV (162 198 cm^{-1}) after taking into account the experimental uncertainties.

At the high-energy side of the PFI−PE band for $C^2\Sigma^+(0_0^0)$, several progressions associated with ν_1^+, ν_2^+, and ν_3^+ modes are observed. The pure ν_1^+ progression includes the bands $^2\Sigma^+(1_0^1)$ at 20.2598 eV, $^2\Sigma^+(1_0^2)$ at 20.4145 eV, and $^2\Sigma^+(1_0^3)$ at

20.5611 eV. The vibration due to the excitation of the ν_2^+ mode consists of the bands $^2\Pi(2_0^1)$ at 20.1645 eV and $^2\Sigma^+(2_0^2)$ at 20.2244 eV. The observation of forbidden transition $^2\Pi(2_0^1)$ can be partially explained by the small deviations from the linear structure.[25] The excitations of the ν_3^+ mode are observed at 20.3899 eV as $^2\Sigma^+(3_0^1)$ and 20.6766 eV as $^2\Sigma^+(3_0^2)$. The frequencies for $N_2O^+(C^2\Sigma^+)$ can be determined from these assignments as $\nu_1^+ = 482$ cm^{-1}, $\nu_2^+ = 1251$ cm^{-1}, and $\nu_3^+ = 2300$ cm^{-1}. The previous HeI measurement reports $\nu_1^+ = 508$ cm^{-1}, $\nu_2^+ = 1242$ cm^{-1}, and $\nu_3^+ = 2282$ cm^{-1}. We note the ν_1^+ and $2\nu_2^+$ bands may interact with each other due to the Fermi resonance; however, the $(0,2,0)C^2\Sigma^+$ state is quite harmonic; thus no significant Fermi resonance interactions would be expected.

The other PFI−PE bands include combination excitations of ν_1^+,ν_2^+ and ν_3^+, e.g. $^2\Pi(1_0^12_0^1)$ at 20.3202 eV, $^2\Sigma^+(1_0^12_0^2)$ at 20.3771 eV, $^2\Sigma^+(2_0^23_0^1)$ at 20.5088 eV, and $^2\Sigma^+(1_0^13_0^1)$ at 20.5406 eV. Table 2 also lists several hot bands, due to the thermal excitation of the ν_2'' mode in the neutral molecule.

IV. Conclusions

A vacuum-UV PFI−PE measurement of N_2O has been performed in the energy region of 16.3−21.0 eV, covering the formation of $N_2O^+(A^2\Sigma^+, \nu_1^+ = 0-4, \nu_2^+ = 0-2$, and $\nu_3^+ = 0-2)$, $N_2O^+(B^2\Pi)$, and $N_2O^+(C^2\Sigma^+, \nu_1^+ = 0-3, \nu_2^+ = 0-2$, and $\nu_3^+ = 0-2)$. The vibronic bands for $N_2O^+(A^2\Sigma^+$ and $C^2\Sigma^+)$ correspond to excitation of the ν_1^+, ν_2^+, and ν_3^+ modes in both odd and even quanta. Many vibronic bands, which were not resolved in previous HeI and TPE studies, are identified in the present PFI−PE measurement. The BOS simulation of the high-resolution PFI−PE bands associated with excitation to $N_2O^+(A^2\Sigma^+, \nu_1^+ = 0-1, \nu_2^+ = 0$, and $\nu_3^+ = 0-1)$ from $N_2O(X^1\Sigma^+)$ was made, yielding accurate IEs for the formation of $A^2\Sigma^+(0_0^0)$, $A^2\Sigma^+(1_0^1)$, $A^2\Sigma^+(3_0^1)$, and $A^2\Sigma^+(1_0^13_0^1)$. Similar to the observation in the previous HeI study, the PFI−PE spectrum in the energy region of 17.3−20.0 eV contains complicated features for $N_2O^+(B^2\Pi)$.

Acknowledgment. The authors thank Dr. C.-W. Hsu, Dr. M. Evans, and Dr. S. Stimson for their help in obtaining PFI−PE data for this system. This work was supported by the U.S. Department of Energy, Office of Basic Energy Sciences, Division of Chemical Sciences, Geosciences, and Biosciences. C.Y.N. also acknowledges support by the NSF Grant ATM001644 and AFOSR Grant No. 49620-99-1-0234 (technical monitor: Dr. Michael Berman).

References and Notes

(1) Duncan, A. B. F. *J. Chem. Phys.* **1936**, *4*, 638.
(2) Tanaka, Y.; Jursa, A. S.; Leblanc, F. J. *J. Chem. Phys.* **1960**, *32*, 1205.
(3) Lindholm, E. *Ark. Fys.* **1969**, *40*, 129.
(4) Danis, P. O.; Wyttenbach, T.; Maier, J. P. *J. Chem. Phys.* **1988**, *88*, 3451.
(5) Shaw, D. A.; Holland, D. M. P.; MacDonald, M. A.; Hopkirk, A.; Hayes, M. A.; McSweeney, S. M. *Chem. Phys.* **1992**, *163*, 387.
(6) Callomon, J. H.; Creutzberg, F. *Philos. Trans. R. Soc. London* **1974**, *277*, 157.
(7) Eland, J. H. D.; Devoret, W.; Leach, S. *Chem. Phys. Lett.* **1976**, *43*, 97.
(8) Maier, J. P.; Thommen, F. *Chem. Phys.* **1980**, *51*, 319.
(9) Aarts, J. F. M.; Callomon, J. H. *Mol. Phys.* **1987**, *62*, 637.
(10) Larzillière, M.; Jungen, CH. *Mol. Phys.* **1989**, *67*, 807.
(11) Chafik el Idriss, M.; Larziliere, M.; Carré, M. *J. Chem. Phys.* **1994**, *100*, 204.
(12) Al-Joboury, M. I.; May, D. P.; Turner, D. W. *J. Chem. Soc.* **1965**, 6350.
(13) Turner D. W.; May, D. P. *J. Chem. Phys.* **1967**, *46*, 1156.
(14) Brundle, C. R.; Turner, D. W. *Int. J. Mass Spectrom. Ion Phys.* **1969**, *2*, 195.
(15) Natalis, P.; Collin, J. E. *Int. J. Mass Spectrom. Ion Phys.* **1969**, *2*, 221.
(16) Carlson, T. A.; McGuire, G. E. *J. Electron Spectrosc. Relat. Phenom.* **1972/1973**, *1*, 209.
(17) Weiss, M. J. *Chem. Phys. Lett.* **1976**, *39*, 250.
(18) Dehmer, P. M.; Dehmer, J. L.; Chupka, W. A. *J. Chem. Phys.* **1980**, *73*, 126.
(19) Cvitaš, T.; Klasinc, L.; Kovač, B.; McDiarmid, R. *J. Chem. Phys.* **1983,** *79*, 1565.
(20) Locht, R.; Caprace, G.; Momigny, J. *Chem. Phys. Lett.* **1984**, *111*, 560.
(21) Frey, R.; Gotchev, B.; Peatman, W. B.; Pollak, H.; Schlag, E. W. *Chem. Phys. Lett.* **1978**, *54*, 411.
(22) Chiang S.; Ma, C. *J. Phys. Chem. A* **2000**, *104*, 1991.
(23) Wiedmann, R. T.; Grant, E. R.; Tonkyn, R. G.; White, M. G. *J. Chem. Phys.* **1991**, *95*, 746.
(24) Kong, W.; Rodgers, D.; Hepburn, J. W. *Chem. Phys. Lett.* **1994**, *221*, 301.
(25) Berkowitz, J.; Eland, J. H. D. *J. Chem. Phys.* **1977**, *67*, 2740.
(26) Hitchcock, A. P.; Brion, C. E.; Van Der Wiel, M. J. *Chem. Phys.* **1980**, *45*, 461.
(27) Lee, L. C.; Carlson, R. W.; Judge, D. L.; Ogawa, M. *J. Phys. B* **1975**, *8*, 977.
(28) Ukai, M.; Kameta, K.; Machida, S.; Kouchi, N.; Hatano, Y.; Tanaka, K. *J. Chem. Phys.* **1994**, *101*, 5473.
(29) Nenner, I.; Guyon, P. M.; Baer, T.; Govers, T. R. *J. Chem. Phys.* **1980**, *72*, 6587.
(30) Richard-Viard, M.; Atabek, O.; Dutuit, O.; Guyon, P. M. *J. Chem. Phys.* **1990**, *93*, 8881.
(31) Kinmond, E.; Eland, J. H. D.; Karlsson, L. *Int. J. Mass Spectrosc.* **1999**, *185/186/187*, 437.
(32) Hikosaka, Y.; Eland, J. H. D. *Chem. Phys.* **2002**, *281*, 91.
(33) Hollas, J. M.; Sutherley, T. A. *Chem. Phys. Lett.* **1973**, *21*, 167.
(34) Köppel, H.; Cederbaum, L. S.; Domcke, W. *Chem. Phys.* **1982**, *69*, 175.
(35) Hsu, C. W.; Evans, M.; Ng, C. Y.; Heimann, P. *Rev. Sci. Instrum.* **1997**, *68*, 1694.
(36) Hsu, C.-W.; Lu, K. T.; Evans, M.; Chen, Y. J.; Ng, C. Y.; Heimann, P. *J. Chem. Phys.* **1996**, *105*, 3950.
(37) Heimann, P. A.; Koike, M.; Hsu, C.-W.; Blank, D.; Yang, X. M.; Suits, A. G.; Lee, Y. T.; Evans, M.; Ng, C. Y.; Flaim, C.; Padmore, H. A. *Rev. Sci. Instrum.* **1997**, *68*, 1945.
(38) Stimson, S.; Chen, Y. J.; Evans, M.; Liao, C. L.; Ng, C. Y.; Hsu, C. W.; Heimann, P. *Chem. Phys. Lett.* **1998**, *289*, 507.
(39) Evans, M.; Stimson, S.; Ng, C. Y.; Hsu C.-W.; Jarvis, G. K. *J. Chem. Phys.* **1999**, *110*, 315. Song, Y.; Evans, M.; Ng, C. Y.; Hsu, C.-W.; Jarvis, G. K. *J. Chem. Phys.* **1999**, *111*, 1905. Evans, M.; Stimson, S.; Ng, C. Y.; Hsu, C.-W. *J. Chem. Phys.* **1998**, *109*, 1285. Hsu, C.-W.; Evans, M.; Stimson, S.; Ng, C. Y. *J. Chem. Phys.* **1998**, *108*, 4701. Hsu, C.-W.; Heimann, P.; Evans, M.; Stimson, S.; Fenn, P. T.; Ng, C. Y. *J. Chem. Phys.* **1997**, *106*, 8931.
(40) Jarvis, G. K.; Evans, M.; Ng, C. Y.; Mitsuke, K. *J. Chem. Phys.* **1999**, *111*, 3058. Jarvis, G. K.; Song, Y.; Ng, C. Y. *J. Chem. Phys.* **1999**, *111*, 1937.
(41) Liu, J. B.; Chen, W. W.; Hsu, C.-W.; Hochlaf, M.; Evans, E.; Stimson, S.; Ng, C. Y. *J. Chem. Phys.* **2000**, *112*, 10767.
(42) Liu, J. B.; Hochlaf, M.; Ng, C. Y. *J. Chem. Phys.* **2000**, *113*, 7988.
(43) Liu, J. B.; Chen, W. W.; Hochlaf, M.; Qian, X. M.; Chang, C.; Ng, C. Y. *J. Chem. Phys.* **2003**, *118*, 149.
(44) Liu, J. B.; Hochlaf, M.; Chambaud, G.; Rosmus, P.; Ng, C. Y. *J. Phys. Chem. A* **2001**, *105*, 2183.
(45) Liu, J. B.; Hochlaf, M.; Ng, C. Y. *J. Chem. Phys.* **2003**, *118*, 4487.
(46) Stimson, S.; Evans, M.; Ng, C. Y.; Hsu, C.-W.; Heimann, P.; Destandau, C.; Chambaud, G.; Rosmus, P. *J. Chem. Phys.* **1998**, *108*, 6205.
(47) Chen, W. W.; Hochlaf, M.; Rosmus, P.; He, G. Z.; Ng, C. Y.; *J. Chem. Phys.* **2002**, *116*, 5612.
(48) Carirns, R. B.; Samson, J. A. R. *J. Opt. Soc. Am.* **1966**, *56*, 1568.
(49) Buckingham, A. D.; Orr, B. J.; Sichel, J. M. *Philos. Trans. R. Soc. London, Ser. A* **1970**, *268*, 147.
(50) Herzberg, G. *Molecular Spectra and Molecular Structure I, Spectra of Diatomic Molecules*; Van Nostrand: Princeton, 1950.
(51) Herzberg, G. *Molecular Spectra and Molecular Structure III, Electronic Spectra and Electronic Structure of Polyatomic Molecules*; Krieger: Malabar, FL, 1991.
(52) Merkt, F.; Fielding, H. H.; Softley, T. P. *Chem. Phys. Lett.* **1993**, *203*, 153.